PCCP

ROYAL SOCIETY OF CHEMISTRY

PAPER

View Article Online
View Journal | View Issue

Cite this: *Phys. Chem. Chem. Phys.*, 2022, **24**, 13066

Temperature-dependent kinetics of the atmospheric reaction between CH_2OO and acetone†

Peng-Biao Wang,[a] Donald G. Truhlar,[b] Yu Xia[c] and Bo Long *[ac]

Received 7th March 2022,
Accepted 4th May 2022

DOI: 10.1039/d2cp01118b

rsc.li/pccp

Criegee intermediates are important oxidants produced in the ozonolysis of alkenes in the atmosphere. Quantitative kinetics of the reactions of Criegee intermediates are required for atmospheric modeling. However, the experimental studies do not cover the full relevant range of temperature and pressure. Here we report the quantitative kinetics of CH_2OO + $CH_3C(O)CH_3$ by using our recently developed dual strategy that combines coupled cluster theory with high excitation levels for conventional transition state theory and well validated levels of density functional theory for direct dynamics calculations using canonical variational transition theory including tunneling. We find that the W3X-L//DF-CCSD(T)-F12b/jun-cc-pVDZ electronic structure method can be used to obtain quantitative kinetics of the CH_2OO + $CH_3C(O)CH_3$ reaction. Whereas previous investigations considered a one-step mechanistic pathway, we find that the CH_2OO + $CH_3C(O)CH_3$ reaction occurs in a stepwise manner. This has implications for the modeling of Criegee-intermediate reactions with other ketones and with aldehydes. In the kinetics calculations, we show that recrossing effects of the conventional transition state are negligible for determining the rate constant of CH_2OO + $CH_3C(O)CH_3$. The present findings reveal that the rate ratio between CH_2OO + $CH_3C(O)CH_3$ and OH + $CH_3C(O)CH_3$ has a significant negative dependence on temperature such that the CH_2OO + $CH_3C(O)CH_3$ reaction can contribute as a significant sink for atmospheric $CH_3C(O)CH_3$ at low temperature. The present findings should have broad implications in understanding the reactions of Criegee intermediates with carbonyl compounds and ketones in the atmosphere.

1. Introduction

Criegee intermediates[1] (carbonyl oxides) are formed in the ozonolysis of unsaturated compounds in the atmosphere,[2–11] and they are very important in the atmosphere because they contribute to the formation of OH radicals[12–27] and secondary organic aerosols.[28–37] Criegee intermediates act as oxidants, and their kinetics provide key parameters[38–42] for estimating the oxidative capacity of the atmosphere.[5,38,40–43] However, information about their kinetics is still limited.[27,44–50]

The reaction between CH_2OO (the simplest Criegee intermediate) and acetone ($CH_3C(O)CH_3$) has been investigated by both experimental[51–55] and theoretical[51,55,56] methods. Although Criegee intermediates in the atmosphere react both as hot nascent radicals and as stabilized intermediates, the laboratory data and the present article are devoted only to the stabilized species. Even when stabilized, though, the intermediates are not fully thermalized, and therefore the reaction rates can in principle depend on pressure as well as temperature. The experimental data is summarized in Table 1; it does not include the full tropospheric temperature and pressure range, and it is partially inconsistent.

We consider the CH_2OO + $CH_3C(O)CH_3$ reaction to produce the secondary ozonide P, which is a 1,2,4-trioxolane as shown in Fig. 1; the quantitative results in this figure will be explained in Section 3.1, but we introduce the figure here to make the point that this is a stepwise process. The reaction begins with the formation of the complex CA, which is a seven-membered ring structure formed by the weak interaction between the oxygen atom of $CH_3C(O)CH_3$ and the carbon atom of CH_2OO and the weak interaction between the hydrogen atom of the

[a] *Department of Physics, Guizhou University, Guiyang, 550025, China. E-mail: wwwltcommon@sina.com*
[b] *Department of Chemistry, Chemical Theory Center, and Supercomputing Institute, University of Minnesota, Minneapolis, Minnesota 55455-0431, USA*
[c] *College of Materials Science and Engineering, Guizhou Minzu University, Guiyang 550025, China*

† Electronic supplementary information (ESI) available: We list vibrational-frequency scale factors, rate constants, activation energies, tunneling transmission coefficients, recrossing transmission coefficients, optimized geometries, absolute energies in hartrees, and calculated enthalpy profiles. See DOI: https://doi.org/10.1039/d2cp01118b

Table 1 Experimental rate constants for CH_2OO + $CH_3C(O)CH_3$

T (K)	p (torr)	k (10^{-13} cm^3 molecule^{-1} s^{-1})	Ref.
252	30[a]	13.2 ± 1.0	53
258	30	10.8 ± 0.7	53
273	30[a]	6.8 ± 0.8	53
294	30[a]	4.5 ± 0.4	53
302	30	3.7 ± 0.2	53
311	30[a]	3.3 ± 0.2	53
293	5[b]	3.8 ± 0.6	53
293	100[b]	4.7 ± 0.4	53
293	4	2.3 ± 0.3	51
295	67	4.1 ± 0.4	55
297	760	3.4 ± 0.9	54
298	25[c]	3.0 ± 0.6	52
444	25[c]	0.9 ± 0.2	52
494	25	0.7 ± 0.2	52

[a] In these cases, the rate was also measured at 60 torr; in all such cases the error bars corresponding to the two pressures overlap. The error bar is usually smaller at 30 torr, so we report the rate constants at 30 torr. [b] From the fit. [c] In these cases, the pressure dependence was measured from 4 to 50 torr, and "the difference between the rate coefficients across the measured pressure range of interest is comparable to the uncertainty associated with the individual measurements."

CH_3 group and the terminal oxygen atom of CH_2OO. Then the intermediate complex CA is transformed into intermediate complex CB *via* the transition state TSA. Finally complex CB is converted to P *via* transition state TSB. This mechanism is to be contrasted with previous investigations that did not include CA and TSA.[55,56]

In previous theoretical work on the reaction of CH_2OO with acetone, the electronic structure calculations were done by CCSD(T) and density functional theory. Jalan *et al.*[56] used calculated the enthalpy of activation at 0 K to be −4.9 kcal mol^{-1} by using CCSD(T)-F12a/VTZ-F12//B3LYP/MG3S (sometimes to be abbreviated as (CCSD(T)/TF//B/M). Cornwell *et al.*[55] reported a CBS-QB3[57,58] calculation (a composite method whose highest level is CSSD(T) at a B3LYP geometry) indicating that the enthalpy of activation at 0 K for the CH_2OO reaction with acetone is −4.0 kcal mol^{-1}; however, as discussed in Section 3.1, this calculation appears to be in error. Furthermore, previous investigations have shown that higher excitation levels than CCSD(T) (we call them beyond-CCSD(T) calculations) are necessary for reliable results due to the strong multireference characters of Criegee intermediates.[59–65]

In this article, we use our recently developed dual-level rate-constant strategy[60,66–68] and system-specific quantum Rice–Ramsperger–Kassel theory (SS-QRRK) to obtain rate constants for the CH_2OO + $CH_3C(O)CH_3$ reaction under atmospheric temperature and pressure conditions. We use the W3X-L composite method that goes beyond CCSD(T) as the higher level in the dual-level calculations. The W3X-L calculations were carried out at DF-CCSD(T)-F12b[69]/jun-cc-pVDZ[70] geometries; our previous investigations showed that this combination can yield accurate barrier heights.[61]

2. Theoretical methods and strategies

Electronic structure calculations

For the higher level of the dual-level rate constant calculations, all reactants, intermediates, transition states, and products were optimized, and the vibrational frequencies were calculated by using DF-CCSD(T)-F12b/jun-cc-pVDZ. Single-point energy calculations were then calculated using W3X-L[71] composite method.

To choose the lower level, we tested the MN15-L,[72] M11-L,[73] M06-2X,[74] and M06CR[61] density functionals with the MG3S[75] basis set. We choose M11-L from among these trial functionals because it showed best agreement with the higher-level calculations.

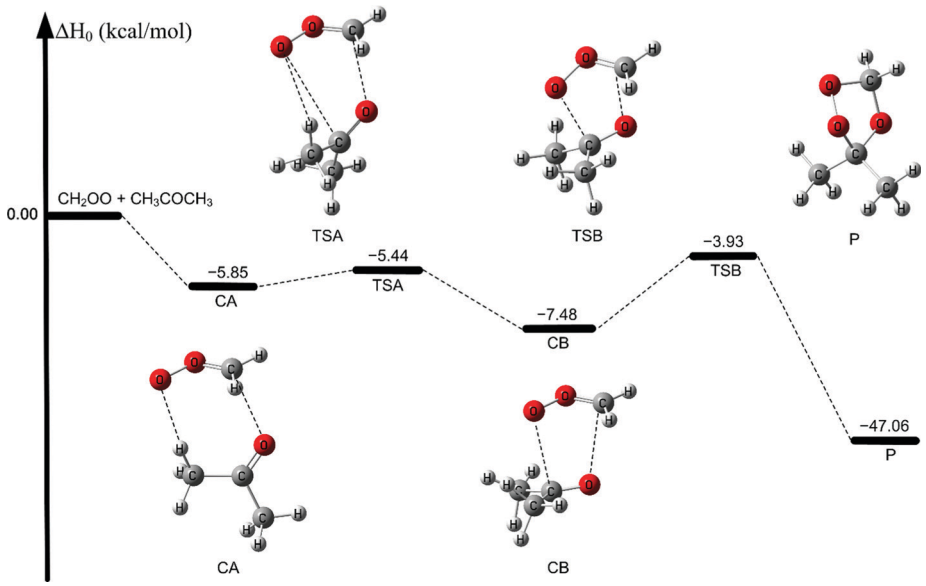

Fig. 1 Enthalpy profile at 0 K for CH_2OO + $CH_3C(O)CH_3$ → P as calculated by W3X-L//DF-CCSD(T)-F12b/jun-cc-pVDZ.

In addition, for comparison, we carried out single-level rate constant calculations with CCSD(T)/TF//B/M and CBS-QB3 because these two methods have been used to investigate the $CH_2OO + CH_3C(O)CH_3$ reaction in the literature.[55,56]

Frequency scaling factors, which are provided in Table S1 (tables and figures with the prefix S are in ESI†), were obtained in a standard way[76] and used to correct systemic errors and include anharmonicity in zero-point vibrational energies.

The electronic structure calculations were performed by using the *Molpro 2019*,[77] *Gaussian 16*,[78] and *MRCC* codes.[79,80]

High-pressure-limit rate constant calculations

The high-pressure-limit rate constant is the rate constant where all species are thermalized. This was calculated by using our dual-level (DL) strategy in which conventional transition state theory without tunneling is done at a high level (HL) and used as a component in canonical variational transition state theory with small-curvature tunneling (CVT/SCT). The CVT/SCT calculation is done by direct dynamics with a more affordable level (lower level, LL). The final rate constant for a given transition state (TSA or TSB) is given by

$$k_{DL}^{CVT/SCT} = \kappa_{LL}\Gamma_{LL}k_{HL}^{\ddagger} \quad (1)$$

where κ_{LL} is the LL tunneling transmission coefficient calculated by the small-curvature tunneling approximation, Γ_{LL} is the LL recrossing transmission coefficient calculated by

$$\Gamma_{LL} = \frac{k_{LL}^{CVT}}{k_{LL}^{\ddagger}} \quad (2)$$

where k_{LL}^{CVT} and $k_{LL}^{\ddagger}$ are respectively the canonical variational transition state theory rate constant and the conventional transition state theory rate constant, and $k_{HL}^{\ddagger}$ is the W3X-L//DF-CCSD(T)-F12b/jun-cc-pVDZ conventional transition state theory rate constant.

Our final estimate of the high-pressure limit rate constants was calculated by the extension of the canonical unified statistical theory[81–84] to the high-pressure limit. For the present application, we ignore the flux through the CA and CB intermediates and the flux through the through the variational transition state between reactants and CA based on the assumption that they are much larger than the fluxes through the TSA and TSB transition states. This assumption gives the rate constant as

$$k = \frac{k_{R\text{-}TSA}^{HP}k_{R\text{-}TSB}^{HP}}{k_{R\text{-}TSA}^{HP} + k_{R\text{-}TSB}^{HP}} \quad (3A)$$

where $k_{R\text{-}TSX}^{HP}$ (X = A or B) is a high-pressure rate constant computed with the bimolecular reactant (R) and the transition state TS*X*. This is given by

$$k_{R\text{-}TSX}^{HP} = K_{R\text{-}CX}k_{CX\text{-}TSX} \quad (3B)$$

We use this notation to emphasize that in the high-pressure limit, one must include tunneling at all energies above the zero-point levels of the complex and the product, whereas in the low-pressure limit one would not include tunneling at all energies above the zero-point levels of the reactant and the product. Notice also that eqn (3A) involves $k_{R\text{-}TSB}^{HP}$, not $k_{CSB\text{-}TSB}^{HP}$.[85]

High-pressure rate constants were calculated by using *Polyrate 2017C*[86] and *Gaussrate 2017B*.[87]

Pressure-dependent rate constant calculations

The pressure dependence was evaluated by the SS-QRRK method[88] and by master equations calculations with the energy-grained master equation (ME) with the direct diagonalization method (diagonalization of the global relaxation matrix to obtain chemically significant eigenmodes[89]). The latter calculations used microcanonical rate constants, which were computed by Rice–Ramsperger–Kassel–Marcus (RRKM) theory[90] with parameters from W3X-L//CCSD(T)/DF-CCSD(T)-F12b/jun-cc-pVDZ. Both sets of calculations indicated that the reaction under study here at temperatures 190–350 K is almost independent of pressure down to pressures of 0.02 bar; therefore we shall not present the pressure-dependent calculations in detail.

The SS-QRRK calculations were carried out with *Polyrate 2017C*,[86] and the RRKM and master equation calculations were done by using the *MESS*[91] program.

3. Results and discussion

3.1. The electronic structures of the $CH_2OO + CH_3C(O)CH_3$ reaction

Fig. 1 shows that transition state TSB is expected to be the rate-determining transition state with an enthalpy of activation (relative to reactants) of −3.93 kcal mol^{-1}, which is 1.51 kcal mol^{-1} higher than that of TSA (−5.44 kcal mol^{-1}). To study the generality of the two-intermediate mechanism, we made calculations for reactions of CH_2OO with $CH_3C(O)CHCH_2$ and CH_3CHO and for reactions of *syn*- and *anti*-CH_3CHOO with $CH_3C(O)CH_3$. The results are in Fig. S1–S4 (ESI†). The important conclusions that may be drawn from these additional calculations are as follows. First, we find that each of these additional reactions has two intermediates, showing that the stepwise mechanism considered here should be widespread in reactions of Criegee intermediates with aldehydes and ketones. Second, Fig. S2 (ESI†) shows that in terms of enthalpy of activation, the first transition state is the rate-determining step in the $CH_2OO + CH_3CHO$. Thus, although TSA is not rate-determining for $CH_2OO + CH_3C(O)CH_3$, we find that it can be rate-determining for other reactions of this type.

Table 2 shows that the mean unsigned derivation (MUD) of W2X, which is a CCSD(T)/CBS-level method, from W3X-L, which is a CCSDT(Q)/CBS-level method, is 0.46 kcal mol^{-1}; this shows that beyond-CCSD(T) calculations are necessary for obtaining accurate reaction energetics for this kind of reaction. We were unable to find a density functional that attains an accuracy as high as W2X, but Table 2 shows that the M11-L/MG3S density functional method has an MUD of only 0.65 kcal mol^{-1}, which is even better than CCSD(T)/TF//B/M. Therefore, we chose M11-L/MG3S to do the direct dynamics calculations.

Table 2 Calculated enthalpies at 0 K (ΔH_0 in kcal mol^{-1}, relative to the bimolecular reactants) and enthalpies of activation at 0 K ($\Delta H_0^{\ddagger}$ in kcal mol^{-1}, relative to the bimolecular reactants) relative the enthalpy of the reactants and mean unsigned deviation (MUD) from best estimate

	ΔH_0	$\Delta H_0^{\ddagger}$	ΔH_0	$\Delta H_0^{\ddagger}$	ΔH_0	
Method	CA	TSA	CB	TSB	P	MUD
W3X-L[a]	−5.85	−5.44	−7.48	−3.93	−47.06	0.00
W2X[a]	−5.98	−5.56	−7.68	−4.41	−48.44	0.46
M11-L/MG3S	−5.24	−4.97	−6.90	−3.53	−45.85	0.65
CCSD(T)-F12a/VTZ-F12[b]	−6.11	−5.74	−7.66	−4.80	−49.04	0.72
M06CR/MG3S	−6.15	−5.82	−7.83	−2.20	−44.35	1.09
CBS-QB3	−6.29	−6.14	−8.32	−6.08	−50.34	1.48
MN15-L/MG3S	−7.08	−6.82	−9.66	−6.08	−47.77	1.53
M06-2X/MG3S	−7.75	−7.19	−10.19	−6.64	−54.55	3.31[c]

[a] Geometries and frequencies by DF-CCSD(T)-F12b/jun-cc-pVDZ. [b] Geometries and frequencies by B3LYP/MG3S. [c] M06-2X has never been recommended for applications to multireference systems like the present one, and the M06-2X results are included here just as a reminder of that fact.

The enthalpy of activation (0 K) of the rate-determining transition state TSB is computed to be −4.8 kcal mol^{-1} in our CCSD(T)/TF//B/M calculation and −4.9 kcal mol^{-1} in the one in the literature[56]); these values are different from our best estimate by 0.9–1.0 kcal mol^{-1}. Such an error in calculating the Boltzmann factor of a transition state would change a predicted rate constant by a factor of 6 or 7 at 250 K. Table 2 shows that the CBS-QBS calculations have an even larger MUD, *i.e.*, 1.5 kcal mol^{-1}. Moreover, the enthalpy of activation (0 K) of the determining rate constant TSB is computed to be −6.1 kcal mol^{-1} by CBS-QBS, which is 2.1 kcal mol^{-1} different from the value reported in the literature by the same theoretical method.[55] To aid those who might wish to reproduce our recalculation, we have uploaded the computed output file of our own calculation by this method in ESI.† An error of 2.1 kcal mol^{-1} in calculating the Boltzmann factor of a transition state would change a predicted rate constant by a factor of 70 at 250 K.

3.2. Kinetics

We calculated the pressure-dependent rate constant using the systems-specific quantum Rice Ramsperger Kassel (SS-QRRK)[88] theory for bimolecular reactions with chemical activation. These rate constants, which are listed in Table S2 (ESI†), showed that that the rate constant of the CH_2OO + $CH_3C(O)CH_3$ reaction is almost independent of pressure; this is consistent with experimental results that the rate constant of CH_2OO + $CH_3C(O)CH_3$ is slightly dependent on pressure.[52] Therefore, we consider the rate constant of CH_2OO + $CH_3C(O)CH_3$ as being dependent only on temperature.

Table 3 provides the rate constants in the CUS expression, and details of these rate constants are given in Tables S3 and S4 (ESI†).

We fit the CUS calculation of k as follows:[83]

$$k = 9.43 \times 10^{-17} \times \left\{\frac{T + 52.53}{300}\right\}^{1.656} \exp\left[-\frac{-3.886(T + 52.53)}{1.987212 \times 10^{-3}(T^2 + 52.53^2)}\right] \quad (4)$$

Table 3 Rate constants (k, cm^3 molecule^{-1} s^{-1}) and activation energies (E_a, kcal mol^{-1}) for CH_2OO + $CH_3C(O)CH_3$

T (K)	$k_{R\text{-}TSA}$[a]	$k_{R\text{-}TSB}$[b]	k[c]	E_a[d]
190	1.12×10^{-8}	1.33×10^{-11}	1.33×10^{-11}	−4.46
210	3.24×10^{-9}	4.34×10^{-12}	4.33×10^{-12}	−4.40
230	1.19×10^{-9}	1.75×10^{-12}	1.75×10^{-12}	−4.31
250	5.22×10^{-10}	8.30×10^{-13}	8.28×10^{-13}	−4.22
270	2.64×10^{-10}	4.45×10^{-13}	4.45×10^{-13}	−4.13
290	1.48×10^{-10}	2.64×10^{-13}	2.63×10^{-13}	−4.04
298	1.21×10^{-10}	2.19×10^{-13}	2.18×10^{-13}	−4.00
310	9.10×10^{-11}	1.69×10^{-13}	1.68×10^{-13}	−3.94
330	5.99×10^{-11}	1.15×10^{-13}	1.15×10^{-13}	−3.84
350	4.18×10^{-11}	8.26×10^{-14}	8.24×10^{-14}	−3.75

[a] This dual-level CVT/SCT rate constant of CH_2OO + $CH_3C(O)CH_3$ reaction was calculated by using only TSA, where the reactants are CH_2OO and $CH_3C(O)CH_3$ and tunneling was calculated from CA to CB. [b] This dual-level CVT/SCT rate constant of CH_2OO + $CH_3C(O)CH_3$ reaction was calculated by using only TSB, in which the reactants are CH_2OO and $CH_3C(O)CH_3$ and tunneling was calculated from CB to P. [c] k is the CUS rate constant of eqn (4). [d] E_a is the Arrhenius activation energy computed from the local slope of ln k *vs.* $1/T$.

The temperature-dependent Arrhenius activation energy can be calculated from this by[83]

$$E_a(T') = \frac{E\left(T'^4 + 2T_0T'^3 - T_0^2T'^2\right)}{\left(T'^2 + T_0^2\right)^2} + \frac{nRT'^2}{T' + T_0} \quad (5)$$

where R is the gas constant (1.987 cal mol^{-1} K^{-1}). The activation energies calculated this way are given in Table 3 with more temperatures in Table S5 (ESI†).

The tunneling and recrossing transmission coefficient at TSA and TSB are listed in Tables S3 and S4 (ESI†). For TSA, the tunneling transmission coefficient is within 3% of unity. However, the recrossing transmission coefficient is within 11% of unity over the whole 190–350 K temperature range. The tunneling transmission coefficient is more significant at TSB where tunneling increases the rate by as much as a factor of 1.49; recrossing is within 3% of unity.

The calculated rate constants show a strong negative temperature dependence, decreasing by a factor of 161 from 190 K to 350 K.

Table 4 compares the computed rate constants to experiment. Most of the experimental rates are larger than the theoretical ones, by factors of 1.2–2.0; in one case the

Table 4 Theoretical and experimental rate constants (10^{-13} cm^3 molecule^{-1} s^{-1}) of the CH_2OO + $CH_3C(O)CH_3$ reaction

T (K)	Theory k	Experimental k	Experimental ref.	Expt./theory
252	7.8	13.2 ± 1.0	53	1.7
263	5.5	9.2 ± 0.6	53	1.7
273	4.1	6.8 ± 0.8	53	1.7
283	3.1	5.3 ± 0.7	53	1.7
293	2.5	4.1 ± 0.4	53	1.6
		2.3 ± 0.3	51	0.9
295	2.3	4.1	55	1.8
297	2.2	3.4 ± 0.9	54	1.5
298	2.2	2.6 ± 0.6	52	1.2
311	1.7	3.2 ± 0.2	53	1.9
340	0.97	1.9 ± 0.3	52	2.0

experimental is smaller than the theoretical one by a factor of 0.9. This is very good accuracy for an absolute rate prediction at very low temperature. For example, the factor of 1.7 deviation at 190 K could be caused by an energy change of only 0.2 kcal mol^{-1} in a Boltzmann factor. We conclude that the dual-level method with beyond-CCSD(T) high-level data is capable of better than a factor of 2 accuracy even at low temperature, and we note that the experiments are only consistent with one another with about a factor of 2, so theory is competing well with experiment. Even more significant is that this validates the use of theoretical results when no experiment is available.

3.3. Atmospheric implications

In the atmosphere, it is generally considered that acetone is lost by its reaction with OH radical.[53,92–94] There are extensive investigations on the OH + $CH_3C(O)CH_3$ reaction by both experimental and theoretical methods.[95–97] Eqn (6) compares the CH_2OO + $CH_3C(O)CH_3$ reaction with the OH + $CH_3C(O)CH_3$ reaction to determine the importance of CH_2OO for the sink of $CH_3C(O)CH_3$:

$$v = \frac{k[CH_3COCH_3][CH_2OO]}{k_{OH}[CH_3COCH_3][OH]} = \frac{k[CH_2OO]}{k_{OH}[OH]} \quad (6)$$

where k is the rate constant of CH_2OO + $CH_3C(O)CH_3$, k_{OH} is the rate constant of OH + $CH_3C(O)CH_3$, and [CH_2OO] and [OH] are their concentrations in the atmosphere. For use in eqn (6), the rate constant of OH + $CH_3C(O)CH_3$ is obtained from experimental results in the literature,[98] yielding

$$k_{OH} = 8.8 \times 10^{-12} \exp(-1320/T) + 1.7 \times 10^{-14} \exp(423/T) \quad (7)$$

The ratio v of eqn (6) was calculated as a function of temperature and the concentrations of [CH_2OO] and [OH]. The resulting rate ratio v is given in Fig. 2 and Tables S6, S7 (ESI†); this shows that the rate ratio v has significantly negative dependency because the value of the rate ratio v at 190 K is about 122 time larger than that of the rate ratio v at 350 K. In the atmosphere, the concentrations of OH and CH_2OO vary from in ranges of 10^4–10^6 molecules cm^{-3} and 5×10^4–5×10^5 molecules cm^{-3}.[99–102] Thus, we consider when the low concentration of CH_2OO is estimated to be 5×10^4 molecules cm^{-3} and the high concentration of OH is 10^6 molecules cm^{-3}, the CH_2OO + $CH_3C(O)CH_3$ reaction still contributes to the sink of $CH_3C(O)CH_3$ because the rate ratio v is 0.11 in Table S6 (ESI†) and Fig. 2. In particular, when the OH concentration is lowered to 10^4 molecules cm^{-3}, the CH_2OO + $CH_3C(O)CH_3$ reaction dominates over the OH + $CH_3C(O)CH_3$ reaction with the concentration of CH_2OO (5×10^4 molecules cm^{-3}) under full atmospheric temperatures.

4. Summary

The reaction of CH_2OO with $CH_3C(O)CH_3$ has been investigated by utilizing our recently developed dual-level strategy. We use the W3X-L[71] composite method that goes beyond CCSD(T) to obtain the reaction enthalpies and activation enthalpies of the reaction between CH_2OO and acetone. We also use these best estimates to show that the M11-L[73] functional has high accuracy, a finding that can be helpful for studying similar reactions of Criegee intermediates with carbonyl compounds. The dual-level rate constant calculations employ CVT/SCT with W3X-L//DF-CCSD(T)-F12b/jun-cc-pVDZ as the higher level and M11-L/MG3S as the lower level. We find that there is a stepwise reaction mechanism for the CH_2OO + $CH_3C(O)CH_3$ reaction, in contrast to the usually assumed one-step route that involves only the second of the two transition states considered here, but we find that the consideration of the first step has a negligible effect on the results. We also report calculations indicating that reactions of Criegee intermediates with other aldehydes and ketones also proceed by a two-step mechanism and it may be more important to consider the extra step in some of those cases. Our calculations agree with the

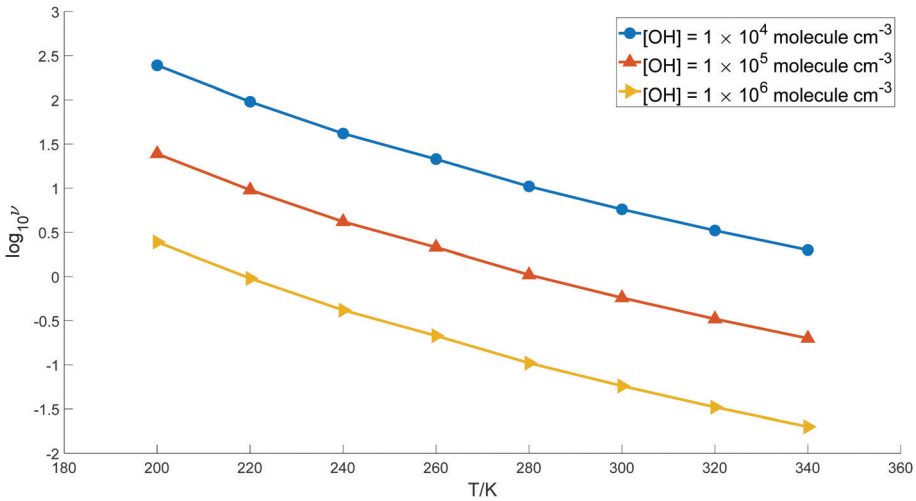

Fig. 2 The rate ratio between CH_2OO + $CH_3C(O)CH_3$ and OH + $CH_3C(O)CH_3$ at different concentrations of OH radical, when the concentration of CH_2OO is 5×10^4 molecule cm^{-3}.

experimental findings that the reaction of CH_2OO with acetone has negative temperature dependence and negligible pressure dependence.

The present findings help to understand the kinetics of CH_2OO + $CH_3C(O)CH_3$ and the sink of $CH_3C(O)CH_3$, and the mechanistic conclusions are relevant for reactions of Criegee intermediates with other aldehydes and ketones.

Conflicts of interest

The authors declare no competing financial interest.

Acknowledgements

The authors thank Junwei Lucas Bao for doing the SS-QRRK calculations. This work was supported in part by the National Natural Science Foundation of China (42120104007, 41775125, and 91961123), by the Science and Technology Foundation of Guizhou Province, China ([2019]5648), by the Science and Technology Foundation of Guizhou Provincial Department of Education, China (KY[2012]014), and by the U.S. Department of Energy, Office of Science, Office of Basic Energy Sciences under Award DE-SC0015997.

References

1 R. Criegee, *Angew. Chem., Int. Ed. Engl.*, 1975, **14**, 745–752.
2 C. Cabezas, M. Nakajima and Y. Endo, *Int. Rev. Phys. Chem.*, 2020, **39**, 349–382.
3 R. Chhantyal-Pun, M. A.-H. Khan, C. A. Taatjes, C. J. Percival, A. J. Orr-Ewing and D. E. Shallcross, *Int. Rev. Phys. Chem.*, 2020, **39**, 383–422.
4 T. A. Stephenson and M. I. Lester, *Int. Rev. Phys. Chem.*, 2020, **39**, 1–33.
5 D. L. Osborn and C. A. Taatjes, *Int. Rev. Phys. Chem.*, 2015, **34**, 309–360.
6 A. S. Hasson, G. Orzechowska and S. E. Paulson, *J. Geophys. Res.*, 2001, **106**, 34131–34142.
7 C. A. Taatjes, *Annu. Rev. Phys. Chem.*, 2017, **68**, 183–207.
8 D. Johnson and G. Marston, *Chem. Soc. Rev.*, 2008, **37**, 699–716.
9 L. Vereecken, *Science*, 2013, **340**, 154–155.
10 C. A. Taatjes, D. E. Shallcross and C. J. Percival, *Phys. Chem. Chem. Phys.*, 2014, **16**, 1704–1718.
11 N. M. Donahue, G. T. Drozd, S. A. Epstein, A. A. Presto and J. H. Kroll, *Phys. Chem. Chem. Phys.*, 2011, **13**, 10848–10857.
12 Y. Fang, F. Liu, V. P. Barber, S. J. Klippenstein, A. B. McCoy and M. I. Lester, *J. Chem. Phys.*, 2016, **144**, 061102.
13 Y. Fang, F. Liu, S. J. Klippenstein and M. I. Lester, *J. Chem. Phys.*, 2016, **145**, 044312.
14 T. L. Nguyen, L. McCaslin, M. C. McCarthy and J. F. Stanton, *J. Chem. Phys.*, 2016, **145**, 131102.
15 Y. Fang, F. Liu, V. P. Barber, S. J. Klippenstein, A. B. McCoy and M. I. Lester, *J. Chem. Phys.*, 2016, **145**, 234308.
16 M. I. Lester and S. J. Klippenstein, *Acc. Chem. Res.*, 2018, **51**, 978–985.
17 A. S. Hansen, Z. Liu, S. Chen, M. G. Schumer, P. J. Walsh and M. I. Lester, *J. Phys. Chem. A*, 2020, **124**, 4929–4938.
18 V. P. Barber, S. Pandit, V. J. Esposito, A. B. McCoy and M. I. Lester, *J. Phys. Chem. A*, 2019, **123**, 2559–2569.
19 P. Rickly and P. S. Stevens, *Atmos. Meas. Tech.*, 2018, **11**, 1–16.
20 A. Novelli, L. Vereecken, J. Lelieveld and H. Harder, *Phys. Chem. Chem. Phys.*, 2014, **16**, 19941–19951.
21 D. Stone, K. Au, S. Sime, D. J. Medeiros, M. Blitz, P. W. Seakins, Z. Decker and L. Sheps, *Phys. Chem. Chem. Phys.*, 2018, **20**, 24940–24954.
22 Y.-L. Li, M.-T. Kuo and J. J.-M. Lin, *RSC Adv.*, 2020, **10**, 8518–8524.
23 L. Vereecken, A. Novelli, A. Kiendler-Scharr and A. Wahner, *Phys. Chem. Chem. Phys.*, 2022, **24**, 6428–6443.
24 V. P. Barber, S. Pandit, A. M. Green, N. Trongsiriwat, P. J. Walsh, S. J. Klippenstein and M. I. Lester, *J. Am. Chem. Soc.*, 2018, **140**, 10866–10880.
25 N. M. Kidwell, H. Li, X. Wang, J. M. Bowman and M. I. Lester, *Nat. Chem.*, 2016, **8**, 509–514.
26 A. M. Green, V. P. Barber, Y. Fang, S. J. Klippenstein and M. I. Lester, *Proc. Natl. Acad. Sci. U. S. A.*, 2017, **114**, 12372–12377.
27 F. Liu, J. M. Beames, A. S. Petit, A. B. Mccoy and M. I. Lester, *Science*, 2014, **345**, 1596–1598.
28 Y. Zhao, L. M. Wingen, V. Perraud and B. J. Finlayson-Pitts, *Atmos. Chem. Phys.*, 2016, **16**, 3245–3264.
29 F. A. Mackenzie-Rae, H. J. Wallis, A. R. Rickard, K. L. Pereira, S. M. Saunders, X. Wang and J. F. Hamilton, *Atmos. Chem. Phys.*, 2018, **18**, 4673–4693.
30 Y. Gong and Z. Chen, *Atmos. Chem. Phys.*, 2021, **21**, 813–829.
31 R. Chhantyal-Pun, M. A.-H. Khan, N. Zachhuber, C. J. Percival, D. E. Shallcross and A. J. Orr-Ewing, *ACS Earth Space Chem.*, 2020, **4**, 1743–1755.
32 Q. Ma, X. Lin, C. Yang, B. Long, Y. Gai and W. Zhang, *R. Soc. open sci.*, 2018, **5**, 172171.
33 Y. Zhao, L. M. Wingen, V. Perraud, J. Greaves and B. J. Finlayson-Pitts, *Phys. Chem. Chem. Phys.*, 2015, **17**, 12500–12514.
34 B. Bonn, G. Schuster and G. K. Moortgat, *J. Phys. Chem. A*, 2002, **106**, 2869–2881.
35 J. Tröstl, W. K. Chuang, H. Gordon, M. Heinritzi, C. Yan, U. Molteni, L. Ahlm, C. Frege, F. Bianchi, R. Wagner, M. Simon, K. Lehtipalo, C. Williamson, J. S. Craven, J. Duplissy, A. Adamov, J. Almeida, A.-K. Bernhammer, M. Breitenlechner, S. Brilke, A. Dias, S. Ehrhart, R. C. Flagan, A. Franchin, C. Fuchs, R. Guida, M. Gysel, A. Hansel, C. R. Hoyle, T. Jokinen, H. Junninen, J. Kangasluoma, H. Keskinen, J. Kim, M. Krapf, A. Kürten, A. Laaksonen, M. Lawler, M. Leiminger, S. Mathot, O. Möhler, T. Nieminen, A. Onnela, T. Petäjä, F. M. Piel, P. Miettinen, M. P. Rissanen, L. Rondo, N. Sarnela, S. Schobesberger, K. Sengupta, M. Sipilä, J. N. Smith, G. Steiner, A. Tomè, A. Virtanen,

A. C. Wagner, E. Weingartner, D. Wimmer, P. M. Winkler, P. Ye, K. S. Carslaw, J. Curtius, J. Dommen, J. Kirkby, M. Kulmala, I. Riipinen, D. R. Worsnop, N. M. Donahue and U. Baltensperger, *Nature*, 2016, **533**, 527–531.

36 M. Kanakidou, J. H. Seinfeld, S. N. Pandis, I. Barnes, F. J. Dentener, M. C. Facchini, R. Van Dingenen, B. Ervens, A. Nenes, C. J. Nielsen, E. Swietlicki, J. P. Putaud, Y. Balkanski, S. Fuzzi, J. Horth, G. K. Moortgat, R. Winterhalter, C. E.-L. Myhre, K. Tsigaridis, E. Vignati, E. G. Stephanou and J. Wilson, *Atmos. Chem. Phys.*, 2005, **5**, 1053–1123.

37 F. Bianchi, J. Tröstl, H. Junninen, C. Frege, S. Henne, C. R. Hoyle, U. Molteni, E. Herrmann, A. Adamov, N. Bukowiecki, X. Chen, J. Duplissy, M. Gysel, M. Hutterli, J. Kangasluoma, J. Kontkanen, A. Kürten, H. E. Manninen, S. Münch, O. Peräkylä, T. Petäjä, L. Rondo, C. Williamson, E. Weingartner, J. Curtius, D. R. Worsnop, M. Kulmala, J. Dommen and U. Baltensperger, *Science*, 2016, **352**, 1109–1112.

38 M. J. Newland, A. R. Rickard, T. Sherwen, M. J. Evans, L. Vereecken, A. Muñoz, M. Ródenas and W. J. Bloss, *Atmos. Chem. Phys.*, 2018, **18**, 6095–6120.

39 C. A. Taatjes, M. A.-H. Khan, A. J. Eskola, C. J. Percival, D. L. Osborn, T. J. Wallington and D. E. Shallcross, *Environ. Sci. Technol.*, 2019, **53**, 1245–1251.

40 D. Meidan, S. S. Brown and Y. Rudich, *ACS Earth Space Chem.*, 2017, **1**, 288–298.

41 C. J. Percival, O. Welz, A. J. Eskola, J. D. Savee, D. L. Osborn, D. O. Topping, D. Lowe, S. R. Utembe, A. Bacak, G. M. Figgans, M. C. Cooke, P. Xiao, A. T. Archibald, M. E. Jenkin, R. G. Derwent, I. Riipinen, D. W.-K. Mok, E. P.-F. Lee, J. M. Dyke, C. A. Taatjes and D. E. Shallcross, *Faraday Discuss.*, 2013, **165**, 45–73.

42 M. A.-H. Khan, W. C. Morris, M. Galloway, B. M.-A. Shallcross, C. J. Percival and D. E. Shallcross, *Int. J. Chem. Kinet.*, 2017, **49**, 611–621.

43 R. L. Mauldin III, T. Berndt, M. Sipilä, P. Paasonen, T. Petäjä, S. Kim, T. Kurtén, F. Stratmann, V.-M. Kerminen and M. Kulmala, *Nature*, 2012, **488**, 193–196.

44 Y.-P. Lee, *J. Chem. Phys.*, 2015, **143**, 020901.

45 Y.-T. Su, H.-Y. Lin, R. Putikam, H. Matsui, M. C. Lin and Y.-P. Lee, *Nat. Chem.*, 2014, **6**, 477–483.

46 W. Chao, J.-T. Hsieh, C.-H. Chang and J. J.-M. Lin, *Science*, 2015, **347**, 751–754.

47 C. A. Taatjes, O. Welz, A. J. Eskola, J. D. Savee, A. M. Scheer, D. E. Shallcross, B. Rotavera, E. P.-F. Lee, J. M. Dyke, D. K. W. Mok, D. L. Osborn and C. J. Percival, *Science*, 2013, **340**, 177–180.

48 Y.-T. Su, Y.-H. Huang, H. A. Witek and Y.-P. Lee, *Science*, 2013, **340**, 174–176.

49 M. A.-H. Khan, C. J. Percival, R. L. Caravan, C. A. Taatjes and D. E. Shallcross, *Environ. Sci.: Process. Impacts*, 2018, **20**, 437–453.

50 R. A. Cox, M. Ammann, J. N. Crowley, H. Herrmann, M. E. Jenkin, V. F. McNeill, A. Mellouki, J. Troe and T. J. Wallington, *Atmos. Chem. Phys.*, 2020, **20**, 13497–13519.

51 C. A. Taatjes, O. Welz, A. J. Eskola, J. D. Savee, D. L. Osborn, E. P.-F. Lee, J. M. Dyke, D. W.-K. Mok, D. E. Shallcross and C. J. Percival, *Phys. Chem. Chem. Phys.*, 2012, **14**, 10391–10400.

52 R. M.-I. Elsamra, A. Jalan, Z. J. Buras, J. E. Middaugh and W. H. Green, *Int. J. Chem. Kinet.*, 2016, **48**, 474–488.

53 R. Chhantyal-Pun, M. A.-H. Khan, R. Martin, N. Zachhuber, Z. J. Buras, C. J. Percival, D. E. Shallcross and A. J. Orr-Ewing, *ACS Earth Space Chem.*, 2019, **3**, 2363–2371.

54 T. Berndt, R. Kaethner, J. Voigtländer, F. Stratmann, M. Pfeifle, P. Reichle, M. Sipilä, M. Kulmala and M. Olzmann, *Phys. Chem. Chem. Phys.*, 2015, **17**, 19862–19873.

55 Z. A. Cornwell, A. W. Harrison and C. Murray, *J. Phys. Chem. A*, 2021, **125**, 8557–8571.

56 A. Jalan, J. W. Allen and W. H. Green, *Phys. Chem. Chem. Phys.*, 2013, **15**, 16841–16852.

57 J. A. Montgomery, Jr., M. J. Frisch, J. W. Ochterski and G. A. Petersson, *J. Chem. Phys.*, 1999, **110**, 2822–2827.

58 J. A. Montgomery, Jr., M. J. Frisch, J. W. Ochterski and G. A. Petersson, *J. Chem. Phys.*, 2000, **112**, 6532–6542.

59 B. Long, J. L. Bao and D. G. Truhlar, *J. Am. Chem. Soc.*, 2016, **138**, 14409–14422.

60 B. Long, J. L. Bao and D. G. Truhlar, *Proc. Natl. Acad. Sci. U. S. A.*, 2018, **115**, 6135–6140.

61 B. Long, Y. Wang, Y. Xia, X. He, J. L. Bao and D. G. Truhlar, *J. Am. Chem. Soc.*, 2021, **143**, 8402–8413.

62 B. Long, J. L. Bao and D. G. Truhlar, *Nat. Commun.*, 2019, **10**, 2003.

63 J. P. Misiewicz, S. N. Elliott, K. B. Moore III and H. F. Schaefer III, *Phys. Chem. Chem. Phys.*, 2018, **20**, 7479–7491.

64 H. F. Mull, G. J.-R. Aroeira, J. M. Turney and H. F. Schaefer III, *Phys. Chem. Chem. Phys.*, 2020, **22**, 22555–22566.

65 G. J.-R. Aroeira, A. S. Abbott, S. N. Elliott, J. M. Turney and H. F. Schaefer III, *Phys. Chem. Chem. Phys.*, 2019, **21**, 17760–17771.

66 X.-F. Tan, B. Long, D.-S. Ren, W.-J. Zhang, Z.-W. Long and E. Mitchell, *Phys. Chem. Chem. Phys.*, 2018, **20**, 7701–7709.

67 B. Long, J. L. Bao and D. G. Truhlar, *J. Am. Chem. Soc.*, 2019, **141**, 611–617.

68 X.-F. Tan, L. Zhang and B. Long, *Phys. Chem. Chem. Phys.*, 2020, **22**, 8800–8807.

69 W. Győrffy and H.-J. Werner, *J. Chem. Phys.*, 2018, **148**, 114104.

70 T. M. Parker, L. A. Burns, R. M. Parrish, A. G. Ryno and C. D. Sherrill, *J. Chem. Phys.*, 2014, **140**, 094106.

71 B. Chan and L. Radom, *J. Chem. Theory Comput.*, 2015, **11**, 2109–2119.

72 H. S. Yu, X. He and D. G. Truhlar, *J. Chem. Theory Comput.*, 2016, **12**, 1280–1293.

73 R. Peverati and D. G. Truhlar, *J. Phys. Chem. Lett.*, 2012, **3**, 117–124.

74 Y. Zhao and G. D. Truhlar, *Theor. Chem. Acc.*, 2008, **120**, 215–241.

75 B. J. Lynch, Y. Zhao and D. G. Truhlar, *J. Phys. Chem. A*, 2003, **107**, 1384–1388.

76 I. M. Alecu, J. Zheng, Y. Zhao and D. G. Truhlar, *J. Chem. Theory Comput.*, 2010, **6**, 2872–2887.

77 H.-J. Werner, P. J. Knowles, G. Knizia, F. R. Manby and M. Schütz, *Wiley Interdiscip. Rev.: Comput. Mol. Sci.*, 2012, **2**, 242–253.
78 M. J. Frisch, G. W. Trucks, H. B. Schlegel, G. E. Scuseria, M. A. Robb, J. R. Cheeseman, G. Scalmani, V. Barone, G. A. Petersson, H. Nakatsuji, X. Li, M. Caricato, A. V. Marenich, J. Bloino, B. G. Janesko, R. Gomperts, B. Mennucci, H. P. Hratchian, J. V. Ortiz, A. F. Izmaylov, J. L. Sonnenberg, D. Williams-Young, F. Ding, F. Lipparini, F. Egidi, J. Goings, B. Peng, A. Petrone, T. Henderson, D. Ranasinghe, V. G. Zakrzewski, J. Gao, N. Rega, G. Zheng, W. Liang, M. Hada, M. Ehara, K. Toyota, R. Fukuda, J. Hasegawa, M. Ishida, T. Nakajima, Y. Honda, O. Kitao, H. Nakai, T. Vreven, K. Throssell, J. A. Montgomery, Jr., J. E. Peralta, F. Ogliaro, M. J. Bearpark, J. J. Heyd, E. N. Brothers, K. N. Kudin, V. N. Staroverov, T. A. Keith, R. Kobayashi, J. Normand, K. Raghavachari, A. P. Rendell, J. C. Burant, S. S. Iyengar, J. Tomasi, M. Cossi, J. M. Millam, M. Klene, C. Adamo, R. Cammi, J. W. Ochterski, R. L. Martin, K. Morokuma, O. Farkas, J. B. Foresman and D. J. Fox, *Gaussian 16, Revision A03*, Gaussian, Inc., Wallingford CT, 2016.
79 M. Kállay, P. R. Nagy, D. Mester, Z. Rolik, G. Samu, J. Csontos, J. Csóka, P. B. Szabó, L. Gyevi-Nagy, B. Hégely, I. Ladjánszki, L. Szegedy, B. Ladóczki, K. Petrov, M. Farkas, P. D. Mezei and A. Ganyecz, *J. Chem. Phys.*, 2020, **152**, 074107.
80 M. Kállay, P. R. Nagy, D. Mester, Z. Rolik, G. Samu, J. Csontos, J. Csóka, P. B. Szabó, L. Gyevi-Nagy, B. Hégely, I. Ladjánszki, L. Szegedy, B. Ladóczki, K. Petrov, M. Farkas, P. D. Mezei and A. Ganyecz, MRCC, A Quantum Chemical Program Suite. **www.mrcc.hu** (accessed 2020-02-22).
81 B. C. Garrett and D. G. Truhlar, *J. Chem. Phys.*, 1982, **76**, 1853–1858.
82 D. G. Truhlar, A. D. Isacson and B. C. Garrett, *Generalized Transition State Theory. In Theory of Chemical ReactionDynamics*, CRC Press, Boca Raton, 1985, vol. 4, pp. 65–137.
83 J. L. Bao and D. G. Truhlar, *Chem. Soc. Rev.*, 2017, **46**, 7548–7596.
84 L. Zhang, D. G. Truhlar and S. Sun, *Proc. Natl. Acad. Sci. U. S. A.*, 2020, **117**, 5610–5616.
85 J. Zheng and D. G. Truhlar, *Faraday Discuss.*, 2012, **157**, 59–88.
86 J. Zheng, J. L. Bao, R. Meana-Pañeda, S. Zhang, B. J. Lynch, J. C. Corchado, Y.-Y. Chuang, P. L. Fast, W.-P. Hu, Y.-P. Liu, G. C. Lynch, K. A. Nguyen, C. F. Jackels, A. Fernandez-Ramos, B. A. Ellingson, V. S. Melissas, J. Villà, I. Rossi, E. L. Coitiño, J. Pu, T. V. Albu, A. Ratkiewicz, R. Steckler, B. C. Garrett, A. D. Issacson and D. G. Truhlar, *Polyrate, version 2017-C*, University of Minnesota, Minneapolis, MN, 2018.
87 J. Zheng, J. L. Bao, S. Zhang, J. C. Corchado, R. Meana-Pañeda, Y.-Y. Chuang, E. L. Coitiño, B. A. Ellingson and D. G. Truhlar, *Gaussrate, version 2017-B*, University of Minnesota, Minneapolis, MN, 2018.
88 J. L. Bao, J. Zheng and D. G. Truhlar, *J. Am. Chem. Soc.*, 2016, **138**, 2690–2704.
89 Y. Georgievskii, J. A. Miller, M. P. Burke and S. J. Klippenstein, *J. Phys. Chem. A*, 2013, **117**, 12146–12154.
90 S. J. Klippenstein, *Comprehensive Chem. Kinet.*, 2003, **39**, 55–103.
91 Y. Georgievskii and S. J. Klippenstein, MESS. **https://tcg.cse.anl.gov/papr/codes/mess.html** (accessed May 1, 2019).
92 M. A.-H. Khan, M. C. Cooke, S. R. Utembe, A. T. Archibald, P. Maxwell, W. C. Morris, P. Xiao, R. G. Derwent, M. E. Jenkin, C. J. Percival, R. C. Walsh, T. D.-S. Young, P. G. Simmonds, G. Nickless, S. O'Doherty and D. E. Shallcross, *Atmos. Environ.*, 2015, **112**, 269–277.
93 H. B. Singh, D. O'Hara, D. Herlth, W. Sachse, D. R. Blake, J. D. Bradshaw, M. Kanakidou and P. J. Crutzen, *J. Geophys. Res.*, 1994, **99**, 1805–1819.
94 D. J. Jacob, B. D. Field, E. M. Jin, I. Bey, Q. Li, J. A. Logan and R. M. Yantosca, *J. Geophys. Res.*, 2002, **107**, ACH 5-1–ACH 5-17.
95 M. Wollenhaupt, S. A. Carl, A. Horowitz and J. N. Crowley, *J. Phys. Chem. A*, 2000, **104**, 2695–2705.
96 T. Yamada, P. H. Taylor, A. Goumri and P. Marshall, *J. Chem. Phys.*, 2003, **119**, 10600–10606.
97 T. J. Wellington and M. J. Kurylo, *J. Chem. Phys.*, 1987, **91**, 5050–5054.
98 R. Atkinson, D. L. Baulch, R. A. Cox, J. N. Crowley, R. F. Hampson, R. G. Hynes, M. E. Jenkin, M. J. Rossi and J. Troe, *Atmos. Chem. Phys.*, 2006, **6**, 3625–4055.
99 A. Novelli, K. Hens, C. T. Ernest, M. Martinez, A. C. Nölscher, V. Sinha, P. Paasonen, T. Petäjä, M. Sipilä, T. Elste, C. Plass-Dülmer, G. J. Phillips, D. Kubistin, J. Williams, L. Vereecken, J. Lelieveld and H. Harder, *Atmos. Chem. Phys.*, 2017, **17**, 7807–7826.
100 F. Rohrer and H. Berresheim, *Nature*, 2006, **442**, 184–187.
101 S. Gligorovski, R. Strekowski, S. Barbati and D. Vione, *Chem. Rev.*, 2015, **115**, 13051–13092.
102 B. Long, J. L. Bao and D. G. Truhlar, *Phys. Chem. Chem. Phys.*, 2017, **19**, 8091–8100.